

# Present-Day Growth of Black Holes and Bulges: the SDSS Perspective

Timothy M. Heckman<sup>1</sup>, Guinevere Kauffmann<sup>2</sup>, Jarle Brinchmann<sup>2,3</sup>, Stéphane Charlot<sup>2,4</sup>,  
Christy Tremonti<sup>5</sup> and Simon D.M. White<sup>2</sup>

heckman@pha.jhu.edu, gamk@mpa-garching.mpg.de

## ABSTRACT

We investigate the accretion-driven growth of supermassive black holes in the low-redshift Universe using 23,000 narrow-emission-line (“Type 2”) active galactic nuclei (AGN) and the complete sample of 123,000 galaxies in the Sloan Digital Sky Survey from which they were drawn. We use the stellar velocity dispersions of the early type galaxies and AGN hosts to estimate their black hole masses and we use the AGN [OIII] $\lambda$ 5007 emission line luminosities to estimate black hole accretion rates. We find that most present-day accretion occurs onto black holes with masses less than  $10^8 M_\odot$  that reside in moderately massive galaxies ( $M_* \sim 10^{10}$  to  $10^{11.5} M_\odot$ ) with high stellar surface mass densities ( $\mu_* \sim 10^{8.5}$  to  $10^{9.5} M_\odot \text{ kpc}^{-2}$ ) and young stellar populations. The volume-averaged accretion rates of low mass black holes ( $< 3 \times 10^7 M_\odot$ ) imply that this population is growing on a timescale that is comparable to the age of the Universe. Around half this growth takes place in AGN that are radiating within a factor of five of the Eddington luminosity. Such systems are rare, making up only 0.2 % of the low mass black hole population at the present day. The rest of the growth occurs in lower luminosity AGN. The growth timescale is more than two orders of magnitude longer for the population of the most massive black holes in our sample. The volume-averaged ratio of star formation to black hole accretion in bulge-dominated galaxies is  $\sim 1000$ , in remarkable agreement with the observed ratio of stellar mass to black hole mass in nearby galaxy bulges. We conclude:

---

<sup>1</sup>Center for Astrophysical Sciences, Department of Physics & Astronomy, Johns Hopkins University, Baltimore, MD 21218

<sup>2</sup>Max Planck Institut für Astrophysik, D-85748 Garching, Germany

<sup>3</sup>Centro de Astrofísica da Universidade do Porto, Rua das Estrelas, 4150-762 Porto, Portugal

<sup>4</sup>Institut d’Astrophysique du CNRS, 98 bis Boulevard Arago, F-75014 Paris, France

<sup>5</sup> Steward Observatory, 933 North Cherry Ave, Tuscon, AZ 85721

a) that bulge formation and black hole formation are tightly coupled, even in present-day galaxies; and b) that the evolution of the AGN luminosity function documented in recent optical and X-ray surveys is driven by a decrease in the characteristic mass scale of actively accreting black holes.

*Subject headings:* Galaxies: Active, Bulges, Evolution, Nuclei, Stellar Content

## 1. Introduction

Over the past few years there have been remarkable developments in our understanding of active galactic nuclei (AGN) and their role in galaxy formation and evolution. There is now compelling evidence (Miyoshi et al. 1995; Genzel et al. 2000) for the existence of the supermassive black holes that were long hypothesized as the power-source for active galactic nuclei (Salpeter 1964; Lynden-Bell 1969). The local mass density in these black holes is sufficient to have powered the total emission of the AGN population over cosmic time if the accreting material is assumed to radiate with an efficiency near the upper end of the plausible range (Yu & Tremaine 2002; Marconi et al. 2004). The tight correlation between the mass of the black hole and the velocity dispersion and mass of the galactic bulge within which it resides (Ferrarese & Merritt 2000; Gebhardt et al. 2000; Marconi & Hunt 2003) is compelling evidence for a close connection between the formation of the black hole and that of its host galaxy (e.g. Cattaneo et al. 1999; Kauffmann & Haehnelt 2000; Granato et al. 2001). Finally, deep x-ray surveys have recently established that the AGN population exhibits so-called “cosmic down-sizing”: the space density of AGN with low x-ray luminosities peaks at *lower redshift* than that of AGN with high x-ray luminosities (Steffen et al 2003; Ueda et al. 2003). These results indicate that a substantial amount of the total black hole growth has occurred more recently than would have been deduced based on optical surveys of powerful quasars (Boyle et al. 2000; Fan et al. 2001). However, from these surveys alone it is not clear whether this downsizing in luminosity is driven by a decrease of the accretion rate in Eddington units, or by a decrease in the characteristic mass-scale for the actively growing black holes. Breaking this degeneracy requires information about black hole mass.

The co-evolution of galaxies and black holes can be directly investigated through deep surveys spanning a broad range in redshift. In the present paper, however, we take a complementary approach and use the Sloan Digital Sky Survey (SDSS) to examine the relationship between galaxies and their supermassive black holes in the present-day Universe. This paper builds on the results in Kauffmann et al. (2003a: hereafter K03), in which we identified a sample of nearly 23,000 narrow-line AGN in the SDSS and investigated the properties of their host galaxies as a function of AGN luminosity. We found that AGN reside almost

exclusively in massive galaxies with structural properties similar to normal early-type systems. We also found that more powerful AGN are hosted by galaxies with younger mean stellar ages. We interpreted the relation between AGN luminosity and stellar age as saying that if gas is available to fuel the central supermassive black hole, it also forms stars at the same time. In the present paper we seek to understand the implications of these results more deeply by transforming from observables such as AGN luminosity and stellar velocity dispersion, to “physical” quantities such as accretion rate and black hole mass.

In section 2 we briefly review how we use the SDSS spectra and images to measure the key properties of the black holes and of the galaxy population that hosts them. In section 3 we study the properties of black holes that are accreting at the present day, in particular their distributions of mass and of accretion rate in Eddington units. We also study the properties of the host galaxies in which black holes are currently growing, concentrating on their mass, density, structure and star formation rate. In section 4 we conclude with a brief discussion of our results.

## 2. Methodology

### 2.1. The SDSS Data

The data analyzed in this paper are drawn from the Sloan Digital Sky Survey (York et al. 2000; Stoughton et al. 2002). The SDSS is using a dedicated 2.5-meter wide-field telescope at the Apache Point Observatory to conduct an imaging and spectroscopic survey of about a quarter of the sky. The imaging is conducted in the  $u$ ,  $g$ ,  $r$ ,  $i$ , and  $z$  bands (Fukugita et al. 1996; Smith et al. 2002) using a drift scan camera (Gunn et al. 1998). The images are calibrated photometrically (Hogg et al. 2001) and astrometrically (Pier et al. 2003) and are used to select galaxies (Strauss et al. 2002). These are observed with a pair of multi-fiber spectrographs built by Alan Uomoto and his team, with fiber assignment based on an efficient tiling algorithm (Blanton et al. 2003). The data are all spectrophotometrically calibrated using observations of subdwarf F stars in each 3-degree field (Tremonti et al., in prep). Our sample is the same as that described in K03. It is based on spectra of 122,808 galaxies with  $14.5 < r < 17.77$  in the “main” galaxy sample in the publically released SDSS Data Release One (DR1; Abazajian et al 2003).

Our methodology is described in detail in K03, but we briefly summarize it here for the convenience of the reader. We have written special purpose code that fits each SDSS galaxy spectrum with a stellar population model (Bruzual & Charlot 2003) and then subtracts this model to leave a pure emission-line spectrum (Tremonti et al., in prep). Following Baldwin,

Phillips, & Terlevich (1981; hereafter BPT) and Veilleux & Osterbrock (1987), we have identified AGN based on the flux ratios of two pairs of the strongest narrow emission-lines in their optical spectra:  $[\text{OIII}]\lambda 5007/\text{H}\beta$  vs.  $[\text{NII}]\lambda 6584/\text{H}\alpha$  (henceforth the “BPT diagram”). Since our aim is to relate the properties of the AGN to those of their host galaxies, we have excluded objects (Type 1 Seyferts and quasars) in which the AGN themselves contribute significantly to the continuum in the SDSS spectra or images. Using the criteria adopted by K03 leads to a sample of 22,623 narrow-line (Type 2) AGN.

In K03 we found the fraction of galaxies containing weak AGN to decrease with redshift. This is because the projected size of the SDSS 3 arcsec diameter fibers increases with redshift (from  $\sim 3$  kpc to 12 kpc over the range  $z \sim 0.05$  to 0.2). Dilution of AGN emission by increasing amounts of galaxy light then causes us to miss more and more weak systems with increasing redshift. As discussed below, in the present paper we will use the  $[\text{OIII}]\lambda 5007$  emission-line as a proxy for AGN power. The AGN in our sample span a wide range in  $[\text{OIII}]$  luminosity (from roughly  $10^5$  to  $10^{8.5}L_\odot$ ).<sup>1</sup> Based on the tests described in K03, we find that our sample is complete for AGN with  $[\text{OIII}]$  luminosities greater than  $10^6L_\odot$  (we recognize these as AGN even at the outer limit of the survey volume).<sup>2</sup>

## 2.2. Derived Galaxy Properties

As described in Kauffmann et al. (2003b) and Brinchmann et al. (2004 - hereafter B04) we have used the SDSS spectra and images to derive a set of fundamental physical properties for each galaxy. We summarize these now.

We have used two age-sensitive spectral features to characterize the stellar population: the 4000Å break  $D_n(4000)$  and the  $\text{H}\delta$  absorption-line ( $H\delta_A$ ). These indices are compared with a large grid of model galaxy spectra to determine the near-IR (SDSS  $z$ -band) stellar mass-to-light ratio. A comparison of model and observed spectral energy distributions yields a measure of the attenuation of the  $z$ -band luminosity by dust. These parameters are then used to determine the stellar mass ( $M_*$ ) from the  $z$ -band Petrosian magnitude.<sup>3</sup> We also use the Petrosian half-light radius in the  $z$ -band image ( $R_{50}(z)$ ) to measure the effective

---

<sup>1</sup>We use  $H_0 = 70 \text{ km s}^{-1} \text{ Mpc}^{-1}$ ,  $\Omega_M = 0.3$ , and  $\Omega_\Lambda = 0.7$  throughout this paper.

<sup>2</sup>Note that in K03 we used the Balmer decrement to correct the  $[\text{OIII}]$  luminosity for dust extinction. We do *not* make these corrections in the present paper because it complicates the empirical assessment of bolometric corrections, as discussed below.

<sup>3</sup>All stellar masses and star formation rates are based on a Kroupa (2001) initial mass function.

surface mass density  $\mu_* = 0.5M_*/(\pi R_{50}(z))^2$ .

Star formation rates are normally derived for the region sampled by the spectroscopic fiber ( $\text{SFR}_{\text{fib}}$ ) from the extinction-corrected luminosities of the most prominent emission-lines. These lines cannot be used for galaxies with AGN, and  $\text{SFR}_{\text{fib}}$  is instead estimated from  $D_n(4000)$ , based on the strong correlation between  $D_n(4000)$  and specific star-formation rate  $\text{SFR}/M_*$  found for galaxies without AGN. The correction from  $\text{SFR}_{\text{fib}}$  to total star formation rate ( $\text{SFR}_{\text{tot}}$ ) is made using the  $g - r$  and  $r - i$  color of the galaxy in the region outside the fiber. This method exploits the fact that for normal galaxies, the values of these colors measured inside the fiber are a reasonably good predictor of  $\text{SFR}_{\text{fib}}/L_{i,\text{fib}}$  (see B04 for more details). The fiber typically encloses 20% to 50% of the galaxy light.

We use the SDSS concentration index  $C = R_{90}/R_{50}$  (defined as the ratio of the radius enclosing 90% of the total  $r$ -band flux to that enclosing half the  $r$ -band flux) as a measure of galaxy structure. Shimasaku et al. (2001) and Strateva et al. (2001) show that there is a good correspondence between  $C$  and Hubble type, with  $C \sim 2.6$  marking the boundary between early-type galaxies (E,S0 and Sa) and late-type systems (Sb-Irr).

### 2.3. Derived AGN Properties

In this section we discuss how we use the SDSS data to estimate the AGN bolometric luminosity. First we motivate our use of the [OIII] $\lambda$ 5007 emission line luminosity and describe our procedure for correcting it for any contribution from star formation. We then discuss the empirically-based bolometric correction that is applied to the [OIII] luminosity.

#### 2.3.1. The [OIII] Luminosity

We use the luminosity of the [OIII] $\lambda$ 5007 emission-line ( $L_{O3}$ ) as a tracer of AGN activity. This is usually the strongest emission-line in the optical spectra of Type 2 AGN, and it is significantly less contaminated than the others by contributions from star-forming regions. This is important, because the relatively large projected aperture of the SDSS spectra means that such contamination is inevitable.

We have implemented the following procedure to statistically correct  $L_{O3}$  in each AGN for the contribution from star formation. First, we divide the sample of all emission-line galaxies in K03 into three classes, based on location in the BPT diagram (see Figure 1 in K03). AGN-dominated spectra are defined to lie above the demarcation line recommended by Kewley et al. (2001). Normal star forming galaxies are defined to lie below the demarcation

line adopted by K03. “Composite” objects where both an AGN and star formation contribute significantly to the overall emission line spectrum lie between these two lines. We extract all the AGN-dominated and normal star-forming galaxies with stellar masses  $M_* > 10^{10} M_\odot$ . Using these two samples, we then populate the composite region of the BPT diagram by adding the observed line luminosities of each of the AGN in turn to each star-forming galaxies. This creates a population of synthetic objects with  $L_{O3}$  in the range that covers the region of the BPT diagram containing the real composite galaxies. We then bin the synthetic objects according to  $L_{O3}$  and their locations in the BPT diagram. We compute the *average* fractional AGN contribution to  $L_{O3}$  for all the objects in each bin and we use this to correct  $L_{O3}$  for the real composite galaxies that fall in the same bin. The AGN contribution to  $L_{O3}$  ranges from 50% to 90% for the composite objects and is greater than 90% for the AGN-dominated objects.

### 2.3.2. The Bolometric Correction

In the standard paradigm (e.g. Antonucci 1993), AGN can be broadly classified into two groups. In Type 1 objects the central black holes and their associated continuum and broad emission-line regions are viewed directly. In Type 2 objects these regions are obscured along the observer’s line-of-sight by a dusty torus which intercepts the optical and ultraviolet emission and reradiates it in the infrared. The [OIII] $\lambda$ 5007 emission line arises in gas which is photo-ionized by AGN radiation escaping along the polar axis of the torus, but lying well outside the torus. The observed flux is therefore little affected by viewing angle.

We have included only Type 2 AGN in our analysis, because for these objects the AGN itself has no significant impact on our estimation either of the galaxy parameters described above (see K03), or of the black hole mass (see below). Unfortunately the bolometric correction to  $L_{O3}$  for AGN can only be directly determined for Type 1 AGN, where the clear view of the AGN allows the full spectral energy distribution to be measured directly. As just noted, in the standard unified AGN model the [OIII] $\lambda$ 5007 emission-line provides a good indication of the intrinsic luminosity of the AGN in both Type 1 and Type 2 systems. This can be tested by comparing the ratio of the [OIII] flux to the AGN continuum flux for Type 1 and Type 2 AGN in those wavelength regimes where absorption by the torus is least significant and the contribution by starlight is minimal (mid/far infrared, radio, and hard X-ray regimes).

Keel et al. (1994) found that the distributions of the ratio of the infrared (25 and 60  $\mu$ m) to [OIII] fluxes were identical in complete samples of Type 1 and Type 2 AGN selected from the IRAS survey. Similar results were found by Mulchaey et al. (1994) and Heckman (1995)

for independent samples of AGN. The ratio of nonthermal radio continuum to [OIII] is the same in Type 1 and Type 2 AGN to within a factor of two in both radio-quiet (Heckman, 1995) and radio-loud AGN (Simpson 1998). Finally, Mulchaey et al. (1994) showed that the mean ratio of hard X-ray to [OIII] flux is the same in Type 1 and Type 2 AGN. This was later verified by Bassani et al. (1999), so long as Type 2 AGN with Compton-thick tori were excluded. Thus, we will assume that the bolometric correction to  $L_{O3}$  is the same on average in Type 2 and in Type 1 AGN.

We have determined the bolometric correction to  $L_{O3}$  for Type 1 AGN in a two step process. First, we determine the mean ratio of the optical continuum and [OIII] luminosities using the extensive SDSS samples of Type 1 Seyfert nuclei and low-redshift quasars described in Zakamska et al. (2003) and K03. We have merged these two samples and then restricted them to objects with  $z < 0.3$  (our Type 2 AGN have  $\langle z \rangle \sim 0.1$ ). There is a strong linear correlation between  $L_{O3}$  and optical continuum luminosity (see Zakamska et al. 2003), and we find an average ratio  $L_{5000}/L_{O3} \sim 320$  (where  $L_{5000}$  is the monochromatic continuum luminosity  $\lambda P_\lambda$  at 5000 Å rest-frame). The dispersion about this mean is 0.34 dex (one  $\sigma$ ). We have confirmed these results using a much smaller sample of nearby Type 1 Seyfert nuclei ( $\langle z \rangle \sim 0.03$ ) compiled by Dahari & De Robertis (1988).

The second step is to then determine the mean ratio of the bolometric and optical continuum luminosities in Type 1 AGN. The mean Type 1 AGN intrinsic spectral energy distribution in Marconi et al. (2004) gives  $L_{Bol}/L_{5000} = 10.9$ . Elvis et al (1994) find a variance in this ratio of 0.16 dex among Type 1 AGN. The implied bolometric correction is then  $L_{Bol}/L_{O3} \sim 3500$ , with a variance of 0.38 dex. We have verified these results using a smaller sample of 28 Type 1 AGN in the Dahari & De Robertis (1988) catalog with good mid-IR, optical, UV, x-ray, and [OIII] fluxes. While the bolometric correction to  $L_{O3}$  will be uncertain by  $\pm 0.38$  dex for any individual AGN, we will be performing integrals over a sample of more than 20,000 AGN, so we need only have a good estimate of the *average* bolometric correction.

It is important to note that the samples used above to calibrate the bolometric correction are dominated by relatively powerful AGN with  $L_{O3} \sim 10^{6.5}$  to  $10^9 L_\odot$ . Since our SDSS sample extends to lower luminosities, we have examined these samples to look for a systematic luminosity dependence in the bolometric correction. Although we find no evidence for such a trend, in the remainder of the paper we will present results based both on our full sample of AGN (all  $L_{O3}$ ) and on the strong AGN alone ( $L_{O3} \geq 10^{6.5} L_\odot$ ). This luminosity cut also effectively excludes the LINER class of Type 2 AGN. Such AGN may well have very different overall spectral energy distributions than the more powerful Seyfert nuclei and quasars (e.g. Ho 2004). Finally, while  $L_{O3}$  is a reasonable proxy for  $L_{bol}$  in the unified model, it does

depend directly on the availability of gas clouds to ionize. Thus, there could be correlations between host galaxy properties and  $L_{bol}/L_{O3}$ .

### 2.3.3. Missing Type 1 AGN

As explained above, our sample explicitly excludes Type 1 AGN. In this paper, we are interested in documenting which black holes are growing and where they are growing. Thus, it is important to keep in mind the limitations resulting from this exclusion.

In the simplest form of the unified model, the Type 1 and Type 2 AGN are drawn from the same parent population of galaxies and differ only in the orientation of the observer’s line-of-sight. If all tori were similar, our results for black hole demographics could simply be scaled upward by the inverse of the Type 2 AGN fraction. The real situation is more complex. Using the same definition of Type 2 AGN as K03, Hao (2003) and Hao et al. (in preparation) find that the fraction of Type 2 AGN in the SDSS is a weak function of AGN luminosity, decreasing from  $\sim 60\%$  to  $\sim 30\%$  over the range  $L_{O3} \sim 10^{5.5}$  to  $10^{8.5}L_{\odot}$ . The unified model then implies that the torus opening angle is a weakly increasing function of AGN luminosity. The implied total volume-averaged correction for missing Type 1 AGN would be a factor of  $\sim 2$ .

## 2.4. Derived Black Hole Properties

We use the observed correlation between black hole mass  $M_{BH}$  and bulge velocity dispersion  $\sigma_*$  (Tremaine et al. 2002)

$$\log M_{BH} = 8.13 + 4.02 \log(\sigma_*/200\text{kms}^{-1}) \quad (1)$$

to derive a black hole mass for galaxies both with and without AGN. A velocity dispersion is automatically measured for each SDSS galaxy by fitting the observed spectrum with a linear combination of galaxy template spectra broadened by a Gaussian kernel (Schlegel et al. in preparation). The instrumental resolution of the SDSS spectra is  $\sigma_{instr} \sim 60$  to  $70 \text{ km s}^{-1}$ , so we restrict our analysis to galaxies with measured values  $\sigma_* \geq 70 \text{ km s}^{-1}$  (corresponding to  $\log M_{BH} \geq 6.3$ ). We do not apply any aperture corrections to the stellar velocity dispersions, because such corrections are small in early-type galaxies in the SDSS (Bernardi et al. 2003).

For the galaxies without an AGN, we restrict our estimates of black hole mass to galaxies with stellar surface mass densities  $\mu_* > 3 \times 10^8 M_{\odot} \text{ kpc}^{-2}$ . As shown by Kauffmann et



al. (2003c), this value of  $\mu_*$  marks the point where the galaxy population undergoes an abrupt transition from disk-dominated galaxies with young stellar populations and ongoing star formation to bulge-dominated “early-type” galaxies. In disk-dominated galaxies, the velocity dispersion measured inside the fiber will not provide an accurate estimate of black hole mass. Note that if we do include galaxies with  $\mu_* < 3 \times 10^8 M_\odot \text{ kpc}^{-2}$ , the integrated mass density in black holes with  $6.3 < \log M_{BH} < 7$  would increase by a factor of  $\sim 2$ . The integrated mass density in more massive black holes would only increase by  $\sim 1.2 - 1.4$ . None of the qualitative conclusions presented in this paper would change. For AGN hosts, we derive a black hole mass even if  $\mu_* < 3 \times 10^8 M_\odot \text{ kpc}^{-2}$  (since the AGN indicates that there is a black hole). As we will show in section 3.2 below, AGN in host galaxies with  $\mu_* < 3 \times 10^8 M_\odot \text{ kpc}^{-2}$  contribute very little to the volume-averaged black hole mass and accretion rates.

Using the bolometric luminosity, we calculate a mass accretion rate  $\dot{M}$  assuming a fiducial value of  $\epsilon = 10\%$  for the radiative efficiency (e.g. Yu & Tremaine 2002). We then use the black hole mass to calculate an Eddington luminosity and associated Eddington ratios ( $L_{bol}/L_{edding} = \dot{M}_{BH}/\dot{M}_{edding}$  for our assumed fixed value of  $\epsilon$ ). On physical grounds, it is likely that the values we have adopted for both the bolometric correction to  $L_{O3}$  and  $\epsilon$  will not be valid at sufficiently low values of accretion in Eddington units (Narayan et al. 1998; Ho 2004). Indeed we see a transition in AGN type from Seyfert to LINER at a value  $L_{bol}/L_{edding} \sim 1\%$  in our sample. Thus, in the remainder of the paper we will present results based both on our full sample of AGN and on only the AGN with  $L_{bol}/L_{edding} \geq 10^{-2}$ . Clearly, if substantial growth in the mass of the present-day black hole population is occurring via accretion with a very low radiative efficiency, we will miss this. However, as discussed by Yu & Tremaine (2002) and Marconi et al. (2004), the local mass density in present-day black holes is sufficient to have powered the total emission of the AGN population over a Hubble time only if the accreting material is assumed to radiate with  $\epsilon$  no smaller than the value we have adopted. The overall contribution to black hole growth by accretion with low radiative efficiency has evidently not been very important.

### 3. Results

In this section we study where accretion onto black holes, as traced by [OIII] emission from Type 2 AGN, is occurring at the present day. As discussed by Ho et al (1997) and K03, 40–50% of massive galaxies have detectable AGN, but [OIII] emission is very weak in most of these systems so their black holes are clearly not growing very rapidly. Because powerful AGN are rare (only 5% of  $10^{11} M_\odot$  galaxies have Type 2 AGN with  $\log L_{O3} > 10^{6.5} L_\odot$ ),

it is more meaningful to work with *volume-averaged* quantities than to present results for individual AGN. Both normal galaxies and AGN in our sample are selected from an  $r$ -band magnitude-limited redshift survey. We can thus follow the standard procedure and weight each galaxy or AGN by  $1/V_{max}$ , where  $V_{max}$  is the volume over which the object would have been detectable (Schmidt 1968; see K03 and Kauffmann et al 2003b for more details). In this way, we are able to compute the integrated [OIII] luminosity from Type 2 AGN per unit stellar mass or per unit black hole mass. Except when noted otherwise, we will perform these volume integrals over *all* galaxies, not just the AGN hosts.

Throughout the rest of the paper we will denote these volume-integrated quantities by scripted symbols to distinguish them from values for individual objects (e.g.  $\mathcal{M}_{BH}$  vs.  $M_{BH}$  and  $\mathcal{L}_{O3}$  vs.  $L_{O3}$ ).

### 3.1. Which Black Holes are Growing?

In the left hand panel of Fig. 1, the long-dashed curve shows how  $\mathcal{M}_{BH}$ , the integrated mass contained in black holes in our sample, is distributed. We have checked that the distribution we compute agrees well with several other recently derived black hole mass functions (see Marconi et al (2004), and references therein). Recall that we can estimate black hole mass for galaxies with stellar velocity dispersions larger than 70 km/s, which corresponds to  $M_{BH} = 10^{6.3}M_{\odot}$ . As can be seen, the bulk of the mass resides in black holes with masses between  $\sim 10^{7.5}$  and  $10^{8.5}M_{\odot}$ . However, the bulk of the Type 2 AGN luminosity is produced by black holes with significantly lower masses. This is illustrated by the solid, dotted, dashed and dashed-dotted curves, which show how the integrated [OIII] luminosity from Type 2 AGN ( $\mathcal{L}_{O3}$ ) is partitioned among black holes of different mass. The dashed line shows the result that is obtained if we integrate over these AGN without correcting the [OIII] luminosities of composite AGN for the contribution from star formation. The solid line shows the result if this correction is included using the procedure described in section 2.3.1. The dotted line shows what happens if we only consider AGN with  $\log L_{O3} > 10^{6.5}L_{\odot}$  and we correct the [OIII] luminosities for star formation. The dashed-dotted line shows the result for AGN with  $\dot{M}_{BH}/M_{eddington} > 10^{-2}$  and correction for star formation. As can be seen, uncertainties in the nature of the bolometric correction have only a small effect on our results. The peak contribution to  $\mathcal{L}_{O3}$  comes from black holes with masses  $\sim 3 \times 10^7 M_{\odot}$ , which is a factor of 3 less than mass at which the contribution to the black hole mass inventory peaks.

The right hand panel of Fig. 1 shows how the integrated [OIII] luminosity from our sample of Type 2 AGN is distributed as a function of  $L_{O3}$ . Above  $10^6 L_{\odot}$ ,  $\mathcal{L}_{O3}$  is spread rather evenly between low-luminosity and high-luminosity systems up to  $L_{O3} \sim 10^8 L_{\odot}$ . The fall-off

below  $10^6 L_\odot$  is caused by incompleteness in our sample of weak AGN at higher redshifts in the SDSS (see Kauffmann et al (2003c) for a detailed discussion). We have examined a low-redshift subset our AGN sample ( $z < 0.04$ ) in order to estimate the effect of this incompleteness. Our tests show show that low luminosity objects ( $L_{O3} = 10^5$  to  $10^6 L_\odot$ ) that are missing from the the full sample plotted in Fig.1 would account for 16% of the total volume-integrated [OIII] emission by all Type 2. We are thus slightly underestimating  $\mathcal{L}_{O3}$ .

In Fig. 2, we plot  $\mathcal{L}_{O3}/\mathcal{M}_{BH}$  as a function of  $\log M_{BH}$ . If we convert  $\mathcal{L}_{O3}$  into a volume-averaged accretion rate using the relations described in section 2, we can recast  $\mathcal{L}_{O3}/\mathcal{M}_{BH}$  as a growth time for the population of black holes ( $\mathcal{M}_{BH}/\dot{\mathcal{M}}_{BH}$ ). Fig. 2 shows that the most rapidly growing black holes are those with  $M_{BH} < \text{few} \times 10^7 M_\odot$ , with an implied growth time of only  $\sim 20$  to 40 Gyr (twice the age of the universe). Above this mass, the growth time increases very rapidly to become orders of magnitude longer than the Hubble time. Alternatively, we can think of  $\dot{\mathcal{M}}_{BH} t_{Hubble}/\mathcal{M}_{BH}$  as a measure of the ratio of the current to the past-averaged growth rate of black holes. Our results indicate that for low-mass black holes, this is around a half, just for growth associated with Type 2 AGN alone. In contrast, the population of more massive black holes ( $> 10^8 M_\odot$ ) must have formed at significantly higher redshifts, as they are currently experiencing very little additional growth.

One might ask whether  $\mathcal{L}_{O3}/\mathcal{M}_{BH}$  is systematically overestimated for low mass black holes because we have excluded low-density, disk-dominated galaxies in our estimates of integrated black hole mass. We have tested the importance of this effect by placing a black hole with mass given by equation (1) in all galaxies with  $\sigma > 70 \text{ km s}^{-1}$ , irrespective of stellar surface density. We find that this only increases the growth times of the lowest mass black hole population in our sample by a factor of 1.6.

As well as looking at the integrated accretion onto black holes of given mass, it is also interesting to study the *distribution* of accretion rates in these systems. This is shown in Fig. 3. We normalize the accretion rate by dividing by the Eddington rate for each object. The left panel shows the cumulative fraction of black holes that are accreting above a given rate. Results are shown for different ranges in black hole mass, with mass increasing from the solid curve on the right ( $3 \times 10^6 M_\odot$ ) to the dotted curve on the left ( $10^9 M_\odot$ ) by a factor of 3 in each case. Note that the sample has been restricted to AGN with  $\log L_{O3} > 10^{6.5} L_\odot$  (with a correction for the contribution to  $L_{O3}$  from star formation). Thus, we are able to go further down in  $\dot{M}_{BH}/\dot{M}_{edding}$  for more massive black holes. Fig. 3 shows that the accretion rate functions cut off fairly neatly at  $\dot{M}_{BH}/\dot{M}_{edding} \sim 1$ . This gives us confidence that our conversions from  $L_{O3}$  to accretion rate and from  $\sigma$  to black hole mass are yielding reasonable answers. There are more low mass black holes than high mass black holes with very large accretion rates near the Eddington limit. Roughly 0.5 percent of black holes

with  $M_{BH} = 10^7 M_\odot$  are accreting above a tenth the Eddington limit. For black holes with  $M_{BH} \sim 3 \times 10^8 M_\odot$ , the fraction accreting above a tenth Eddington has dropped to  $10^{-4}$ . This explains the exceptionally rapid decline (Figure 2) in  $\mathcal{L}_{O3}/\mathcal{M}_{BH}$  above  $\log M_{BH} \sim 8.6$  for the sample in which we exclude AGN with  $L_{bol}/L_{edding} < 1\%$  (the dot-dash line style).

The right panel of Figure 3 shows the cumulative fraction of the total accreting mass (as traced by Type 2 AGN with  $\log L_{O3} > 10^{6.5} L_\odot$ ) as a function of  $\dot{M}_{BH}/\dot{M}_{edding}$ . Results are shown for low mass black holes with  $M_{BH} < 3 \times 10^7 M_\odot$  (solid) and for high mass black holes with  $M_{BH} > 3 \times 10^7 M_\odot$  (dashed). As can be seen, much of the black hole growth is occurring in systems with high Eddington ratios. For low mass black holes, 50% of all growth occurs in AGN that are within a factor of  $\sim 5$  of the Eddington luminosity. For high mass black holes, half of the present-day growth occurs in AGN radiating above  $\sim 8\%$  Eddington. Yu & Tremaine (2002) have shown that the mass density in black holes estimated from integrating the luminosity function of quasars over all cosmic epochs agrees rather well with the total mass density in black holes in galaxies at the present day. Their analysis did not include low-luminosity or Type 2 AGN and it has thus been something of a puzzle why these two estimates of black hole mass density should agree so well. Our analysis demonstrates that although low-luminosity AGN are numerous, their contribution to the growth of black holes is not dominant.

### 3.2. Where are Black Holes Growing?

In Fig. 4, we plot the integrated [OIII] luminosity from Type 2 AGN binned up as a function of stellar mass  $M_*$ , of stellar surface mass density  $\mu_*$ , of concentration index  $C$  and of 4000 Å break strength  $D_n(4000)$ . Fig. 4 shows that most present-day accretion is taking place in galaxies with young stellar ages ( $D_n(4000) < 1.6$ ), intermediate stellar masses ( $10^{10}$ – $10^{11} M_\odot$ ), high surface mass densities ( $3 \times 10^8 - 3 \times 10^9 M_\odot \text{ kpc}^{-2}$ ), and intermediate concentrations ( $C \sim 2.2$  to  $3.0$ ). K03 already showed that powerful Type 2 AGN occur in galaxies with young stellar populations, so it is no surprise that most of the [OIII] emission comes from galaxies with low values of  $D_n(4000)$ . It is quite remarkable, however, that the [OIII] emission from AGN peaks so near the *transition values* of  $M_*$ ,  $C$  and  $\mu_*$  where the galaxy population switches abruptly from young, star-forming and disk-dominated to old, quiescent and bulge-dominated (Kauffmann et al 2003c).

### 3.3. Bulge building: the relation between star formation and accretion onto black holes

In section 3.2, we showed that the population of low mass black holes is still growing rapidly (at one half of the past-averaged rate, even ignoring the contribution of Type 1 AGN). If the very tight relation between black hole mass and bulge mass is to be maintained, the host bulges of these systems must be “forming” at a comparable rate.

In Fig. 5, we plot  $\mathcal{SFR}/\dot{\mathcal{M}}_{\mathcal{BH}}$ , the ratio of the integrated star formation rate in *all* galaxies to the integrated accretion rate onto black holes, as traced by [OIII] emission from Type 2 AGN. The thick black line shows the result if one considers only the SFR inside the SDSS fiber aperture. The thin black line shows the result using our estimates of *total* SFR (see section 2.2). The dashed lines include all AGN, but with the contribution to  $L_{O3}$  from star formation removed. The solid lines show what happens when the sample is restricted to AGN with  $L_{O3} > 3 \times 10^6 L_{\odot}$ . We have chosen to plot  $\mathcal{SFR}/\dot{\mathcal{M}}_{\mathcal{BH}}$  as a function of black hole mass  $M_{BH}$  and of stellar surface mass density  $\mu_*$ .

From Fig. 5 it is clear that black hole growth is closely linked to star formation in the bulge. At low values of  $\mu_*$  characteristic of disk-dominated galaxies, the ratio of  $\mathcal{SFR}/\dot{\mathcal{M}}_{\mathcal{BH}}$  rises steeply. This is because very few of these galaxies host AGN, but there is plenty of star formation taking place in galaxy disks. At values of  $\mu_*$  above  $3 \times 10^8 M_{*} \text{ kpc}^{-2}$ ,  $\mathcal{SFR}/\dot{\mathcal{M}}_{\mathcal{BH}}$  remains roughly constant. Moreover, its value is  $\sim 1000$ , which is in good agreement with the empirically-derived ratio of bulge mass to black hole mass (Marconi & Hunt 2003). Note that the star formation rate estimated within the fiber is likely to underestimate the true star formation rate in the bulge, particularly for the largest and most massive galaxies. Conversely, the total SFR is probably an overestimate, because many galaxies will have star-forming disks. Given the uncertainties in the bolometric correction, in the conversion from  $L_{\text{bol}}$  to black hole accretion rate, in the effect of the missing Type 1 AGN, and in our estimates of SFR, we find it remarkable that  $\mathcal{SFR}/\dot{\mathcal{M}}_{\mathcal{BH}}$  comes out within a factor of a few of the value that is expected from the  $M_{BH}-M_{\text{bulge}}$  relation.

Finally, in Fig. 6 we compare the average growth time of the population of supermassive black holes with the average growth time of the population of galactic bulges. For galaxies with stellar masses in the interval  $(M_*, M_* + \Delta M_*)$  the black hole growth time is estimated by calculating the total mass in black holes ( $\mathcal{M}_{\mathcal{BH}}$ ) and dividing by the accretion rate deduced from the total Type 2 AGN luminosity in [OIII] ( $\mathcal{L}_{O3}$ ). We restrict this sample to AGN with  $L_{O3} > 3 \times 10^6 L_{\odot}$ . The growth time of the bulge is estimated from the ratio of the total stellar mass within the fiber aperture in these systems to the total star formation rate measured inside the fiber. We perform these integrals only over the bulge-dominated normal galaxy population ( $\mu_* > 3 \times 10^8 M_{\odot} \text{ kpc}^{-2}$ ), but include the contribution to black hole growth by

all AGN. As can be seen, the black hole and bulge growth times track each other remarkably closely for galaxies with  $M_* > 10^{10} M_\odot$ . For low mass bulges/black holes, the growth times are of order the Hubble time, but they increase by more than an order of magnitude for massive bulges/black holes. This is consistent with the fact that the smaller bulges in later type galaxies tend to be younger than the larger bulges in earlier type galaxies (Carollo 2004 and references therein).

#### 4. Discussion

We have used a sample of  $\sim 23,000$  AGN, and a complete sample of  $\sim 123,000$  SDSS galaxies from which they were drawn, to investigate the accretion-driven growth of super-massive black holes in the low-redshift universe, and to relate this growth to the properties of the galaxy population. Before discussing our results, we remind the reader of the limitations of our approach, and the assumptions we have made to deal with them.

1. We have used optical emission-line ratios to identify our AGN. If there is a substantial population of accreting black holes in SDSS galaxies that we do not classify as AGN (e.g. Maiolino et al. 2003), we will have missed their contribution to the total black hole growth.
2. We have considered only Type 2 (narrow line) AGN in which the intense radiation from the central accretion disk is completely obscured along our line-of-sight. The effect of the missing Type 1 AGN is relatively small (a factor of  $\sim 2$ ) for our global assessments, but the slow increase in the ratio of Type 1 to Type 2 with increasing AGN luminosity in the SDSS (Hao 2003) means that we systematically underestimate the contribution of more powerful AGN by a factor of a few.
3. We have used the luminosity of the [OIII] $\lambda 5007$  emission line to estimate Type 2 AGN luminosity, assuming that the bolometric correction is the same as for Type 1 AGN. This approach is motivated by the unified model for AGN, and has been empirically validated in the literature.
4. We are complete only for Type 2 AGN with  $L_{O3}$  above  $10^6 L_\odot$ . We estimate this causes us to miss about 16% of the total volume-integrated [OIII] $\lambda 5007$  luminosity from Type 2 AGN.
5. We have calculated black hole accretion rates for an assumed radiative efficiency of 10%. We will undercount accretion that occurs with lower radiative efficiency.

6. We have used the stellar velocity dispersion measured within the central ( $\sim 3$  to 10 kpc diameter) region to estimate the black hole mass, using the  $M_{BH} - \sigma$  relation. We only derive black hole masses for bulge-dominated normal galaxies with  $\mu_* > 3 \times 10^8 M_\odot \text{ kpc}^{-2}$ , but include all the AGN hosts.

Our most surprising result is that the growth time of the population of low mass black holes ( $< 3 \times 10^7 M_\odot$ ) is short (only  $\sim$  two Hubble times, even ignoring the contribution from Type 1 AGN). Although low mass black holes are growing substantially *in the mean* at the present day, only 0.2% of them are growing at the rate which counts for 50% of the fuelling. This implies that strong fuelling events can only last  $\sim 3 \times 10^7 / N$  years if there are  $N$  events per black hole per Hubble time. This implies that the strong accretion phase is a fraction of a characteristic galaxy dynamical time of  $> 10^8$  yr, the shortest timescale over which significant variations in the star formation rate could occur. The correlation between the stellar age of the host galaxy and AGN luminosity found by K03 might then be a consequence of a starburst occurring simultaneously with the maximum accretion phase, followed by a fairly slow tail-off in accretion as the stellar population ages.

By contrast, we find that massive black holes have very long growth times. On average, black holes with masses of  $\sim 10^9 M_\odot$  are currently accreting at a rate that is several orders-of-magnitude lower than their past averaged rate. This population evidently formed early and has evolved little at recent times. This is consistent with inferred black hole masses for high- $z$  quasars (e.g. McLure & Dunlop 2004).

We have also shown that the ratio of the volume-averaged star formation rate to the volume-averaged black hole accretion rate is  $\sim 10^3$  for bulge-dominated galaxies ( $\mu_* > 10^{8.5} M_\odot \text{ kpc}^{-2}$ ). Given the uncertainties in our estimates of the accretion rate, this is remarkably similar to the present ratio of stellar to black hole mass in galaxy bulges. For the population of such galaxies with stellar masses greater than  $10^{10} M_\odot$ , the mean growth time of the black hole and the mean growth time of the surrounding bulge (measured inside the SDSS fiber aperture) are very similar. After volume averaging, the growth of black holes through accretion and the growth of bulges through star formation are thus related at the present time in the same way that they have been related, on average, throughout cosmic history. It seems likely that the processes that established the tight correlation between bulge mass and black hole mass are still operating in low redshift AGN.

These results suggest a picture in which star formation and black hole growth have been moving steadily and in parallel to lower and lower mass scales since a redshift of  $\sim 2$ . This is consistent with the long established fact that at low redshift more massive galaxies tend to have older stellar populations. Surveys of high redshift galaxies have found direct evidence for such an evolutionary pattern, dubbed “cosmic downsizing” by Cowie et al. (1996), in

the star formation properties of galaxies as a function of mass. More recently x-ray surveys (Ueda et al. 2003; Steffen et al 2003) have shown that the peak in the co-moving emissivity of the AGN population occurs at lower and lower redshift for AGN of lower and lower luminosity. These surveys show that a surprisingly large fraction of the total growth of the black hole population has occurred relatively recently in AGN of modest luminosity. For example, Barger et al. (2003) find that over half the x-ray background has been produced by accreting black holes at  $z < 1$ . However, these surveys do not establish whether this is simply due to a decline with time in the average accretion rate (in Eddington units), or rather to a decline in the characteristic mass scale at which black hole growth occurs (true “cosmic downsizing”). Discriminating between these two possibilities requires estimates of the black hole masses. With the superb statistics provided by the SDSS we have been able to show that real downsizing has occurred in the AGN population.

It is particularly intriguing that most black hole growth is currently occurring in galaxies lying so near the values of galaxy mass, density, and concentration where the galaxy population abruptly transitions from low density, disk-dominated systems with ample ongoing star formation to dense, bulge-dominated systems with little star-formation. This may imply that today’s AGN occur in a narrow “habitable zone” with a precipice to the low mass side (no black holes) and an on-coming forest fire at higher masses (no cold interstellar gas for fuel). As we realize that the Era of AGN did not end at high redshift, it seems that we must also admit that this exciting epoch may be finally drawing to a close.

Funding for the creation and distribution of the SDSS Archive has been provided by the Alfred P. Sloan Foundation, the Participating Institutions, the National Aeronautics and Space Administration, the National Science Foundation, the U.S. Department of Energy, the Japanese Monbukagakusho, and the Max Planck Society. The SDSS web site is <http://www.sdss.org/>. The SDSS is managed by the Astrophysical Research Consortium (ARC) for the Participating Institutions. The Participating Institutions are The University of Chicago, Fermilab, the Institute for Advanced Study, the Japan Participation Group, The Johns Hopkins University, Los Alamos National Laboratory, the Max-Planck-Institute for Astronomy (MPIA), the Max-Planck-Institute for Astrophysics (MPA), New Mexico State University, University of Pittsburgh, Princeton University, the United States Naval Observatory, and the University of Washington. SC thanks the Alexander von Humboldt Foundation, the Federal Ministry of Education and Research, and the Programme for Investment in the Future (ZIP) of the German Government for financial support. JB acknowledges the receipt of an ESA post-doctoral fellowship.



## REFERENCES

- Abazaijan, K. et al, 2003, AJ, 126, 2081
- Antonucci, R. 1993, ARA&A,31, 473
- Baldwin, J., Phillips, M. & Terlevich, R. 1981, PASP, 93, 5
- Bassani, L., Dadina, M., Maiolino, R., Salvati, M., Risaliti, G., Della Ceca, R., Matt, G., & Zamorani, G. 1999, ApJS, 121, 473
- Bernardi, M. et al. 2003, AJ, 125, 1817
- Blanton, M.R., Lupton, R.H., Maley, F.M., Young, N., Zehavi, I., Loveday, J. 2003, AJ, 125, 2276
- Boyle, B.J., Shanks, T., Croom, S.M., Smith, R.J., Miller, L., Loaring, N. & Heymans, C., 2000, MNRAS, 317, 1014 308, 77
- Brinchmann, J., Charlot, S., White, S.D.M., Tremonti, C., Kauffmann, G., Heckman, T.M. & Brinkmann, J., 2004, MNRAS, in press
- Bruzual, G., Charlot, S., 2003, MNRAS, 344, 1000
- Carollo, C.M. 2004, Carnegie Observatories Astrophysics Series, Vol. 1: Coevolution of Black Holes and Galaxies, ed. L. Ho (Cambridge: Cambridge University Press), in press (astro-ph/03060321)
- Cattaneo, A., Haehnelt, M. & Rees, M.J. 1999, MNRAS, 308, 77
- Cowie, L.L., Songaila, A., Hu, E.M. and Coheh, J.G. 1996, AJ, 112, 839
- Dahari, O. & Robertis, M.M. 1988, ApJ, 331, 727
- Fan, X. et al. 2001, AJ, 121, 31
- Ferrarese, L. & Merritt, D. 2000, ApJ, 539, L9
- Fukugita, M., Ichikawa, T., Gunn, J.E., Doi, M., Shimasaku, K., Schneider, D.P. 1996, AJ, 111, 1748
- Gebhardt, K. et al 2000, ApJ, 543, L5
- Genzel, R., Pichon, C., Eckart, A., Gerhard, O.E., & Ott, T. 2000, MNRAS, 317, 348

- Granato, G.L., Silva, L., Monaco, P., Panuzzo, P., Salucci, P., De Zotti, G. & Danese, L. 2001, MNRAS, 324, 757
- Gunn, J., Carr, M., Rockosi, C., Sekiguchi, M., Berry, K., Elms, B., de Haas, E., Ivezić, Z. et al. 1998, ApJ, 116, 3040
- Hao, L. 2003, Ph.D. thesis, Princeton University
- Heckman, T.M. 1995, ApJ, 446, 101
- Ho, L.C. 2004, Carnegie Observatories Astrophysics Series, Vol. 1: Coevolution of Black Holes and Galaxies, ed. L. Ho (Cambridge: Cambridge University Press), in press (astro-ph/0401527)
- Ho, L.C., Filippenko, A.V. & Sargent, W.L.W. 1997, ApJS, 112, 315
- Hogg, D., Finkbeiner, D., Schlegel, D., & Gunn, J. 2001, AJ, 122, 2129
- Kauffmann, G. & Haehnelt, M.G. 2000, MNRAS, 311,576
- Kauffmann, G. et al 2003a, MNRAS, 348, 333 (K03)
- Kauffmann, G. et al, 2003b, MNRAS, 341, 33
- Kauffmann, G. et al, 2003c, MNRAS, 341, 54
- Keel, W.C., De Grijp, M.H.K., Miley, G.K., & Zheng, W. 1994, A&A, 283, 791
- Kewley, L., Dopita, M., Sutherland, R., Heisler, C. & Trevena, J. 2001, ApJ, 556, 121
- Lynden-Bell, D. 1969, MNRAS, 143, 167
- Maiolino, R., Comastri, A., Gilli, R., Nagar, N. M., Bianchi, S., Bker, T., Colbert, E., Krabbe, A., Marconi, A., Matt, G., & Salvati, M. 2003, MNRAS, 344, L59
- Marconi, A. & Hunt, L.K., 2003, ApJ, 589, L21
- Marconi, A., Risaliti, G., Gilli, R., Hunt, L., Maiolino, R. & Salvati, M. 2004, MNRAS, in press (astro-ph/0311619)
- McLure, R.J., & Dunlop, J.S. 2004 submitted to MNRAS, astro-ph/0310267
- Miyoshi, M., Moran, J., Herrnstein, J., Greenhill, L., Nakai, N., Diamond, P. & Inoue, M. 1995, Nature, 373, 127

- Mulchaey, J.S., Koratkar, A., Ward, M.J., Wilson, A.J., Whittle, M., Antonucci, R.R.J., Kinney, A.L. & Hurt, T., 1994, ApJ, 436, 586
- Narayan, R., Mahadevan, R., Grindlay, J. E., Popham, R. G., & Gammie, C. 1998, ApJ, 492, 554
- Pier, J.R., Munn, J.A., Hindsley, R.B., Hennessy, G.S., Kent, S.M., Lupton, R.H., Ivezić, Z., 2003, AJ, 125, 1559
- Salpeter, E. 1964, ApJ, 140, 796
- Schmidt, M. 1968, ApJ, 151, 393
- Shimasaku, K. et al, 2001, AJ, 122, 1238
- Simpson, C. 1998, ApJ, 509, 653
- Smith, J.A., et al 2002, AJ, 123, 2121
- Steffen, A.T., Barger, A.J., Cowie, L.L., Mushotsky, R.F. & Yang, Y. 2003, ApJ, 596, L23
- Stoughton, C. et al, 2002, AJ, 123, 485
- Strauss, M., et al 2002, AJ, 124, 1810
- Strateva, I. et al, 2001, AJ, 122, 1861
- Tremaine, S. et al. 2002, ApJ, 574, 740
- Ueda, Y., Masayuki, A., Ohta, K. & Miyaji, T. 2003, ApJ, 598, 886
- Veilleux, S. & Osterbrock, D. 1987, ApJS, 63, 295
- Yu, Q. & Tremaine, S. 2002, ApJ, 335, 965
- York D.G. et al, 2000, AJ, 120, 1579
- Zakamska, N. et al. 2003, AJ, 126, 2125

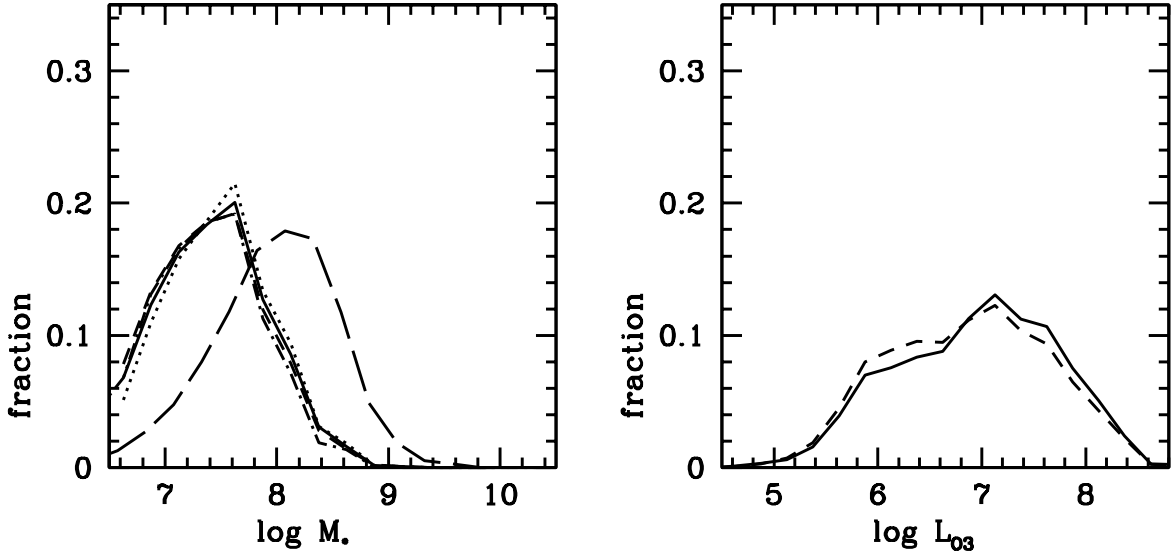


Fig. 1.— Left: The long dashed curve shows the distribution over black hole mass of the volume-weighted total mass of all black holes (active and inactive) in our sample. The solid, dashed, dotted, and dash-dotted lines show the distribution over black hole mass of the volume-weighted total [OIII] luminosity from Type 2 AGN. The dashed line shows the result obtained by integrating over all AGN in the sample. The solid line shows the effect of correcting the [OIII] luminosities for the contribution from star formation. The dotted line shows the result obtained if one only integrates over AGN with  $\log L_{O3} > 10^{6.5} L_{\odot}$  and one also corrects  $L_{O3}$  for star formation. The dashed-dotted line is for AGN with  $\dot{M}/M_{\text{edd}} > 10^{-2}$  and corrected for star formation. Right: The distribution over  $L_{O3}$  for individual AGN of the total volume-weighted [OIII] luminosity from AGN. The solid line shows the result obtained when  $L_{O3}$  is corrected for star formation and the dashed line shows the result without any correction. Note that the decline below  $\log L_{O3} = 10^6 L_{\odot}$  is due to incompleteness in our sample.

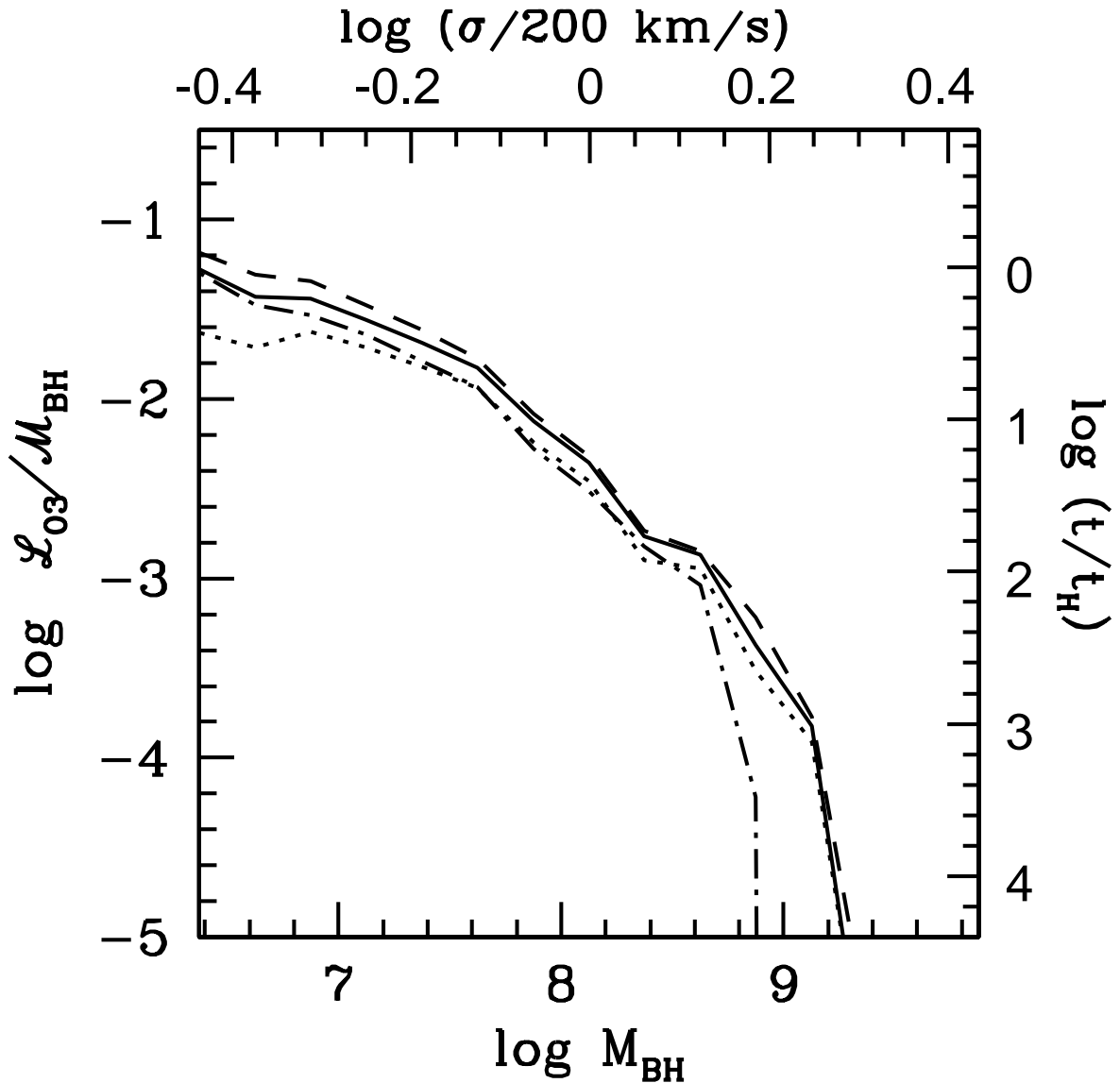


Fig. 2.— The logarithm of the ratio of the total volume-weighted [OIII] luminosity in Type 2 AGN to the total volume-weighted mass in black holes (both in solar units) is plotted as a function of velocity dispersion  $\sigma$  (upper axis) and  $\log M_{BH}$  (lower axis). The right axis shows the corresponding growth time for the population of black holes in units of the Hubble time. The line types are as described in Fig. 1.

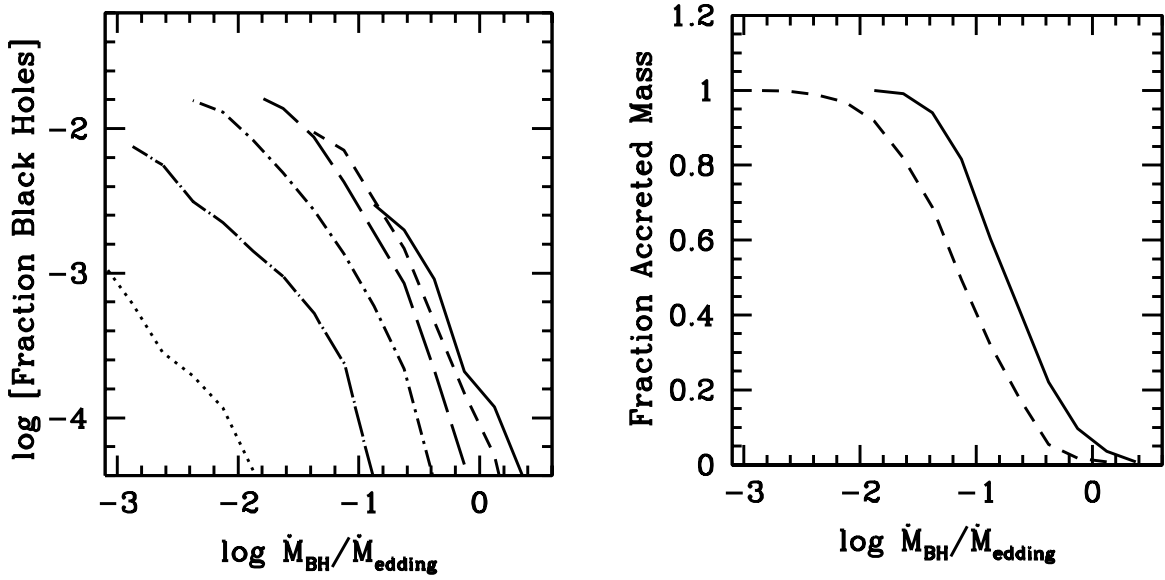


Fig. 3.— Left: The fraction of all black holes accreting above a given rate (in Eddington units). Solid, short-dashed, long-dashed, short dashed-dotted, long dashed-dotted and dotted curves are for black holes with  $3 \times 10^6$ ,  $10^7$ ,  $3 \times 10^7$ ,  $10^8$ ,  $3 \times 10^8$  and  $10^9 M_{\odot}$ , respectively. Right: The cumulative fraction of the total volume-weighted mass accretion rate contributed by Type 2 AGN accreting above a given rate. The solid curve is for black holes with  $M_{\text{BH}} < 3 \times 10^7 M_{\odot}$  and the dashed curve is for black holes with masses above this value. These distributions are all computed for AGN with  $\log L_{\text{O}3} > 10^{6.5} L_{\odot}$  only (with a correction for the contribution of star formation to  $L_{\text{O}3}$ ).

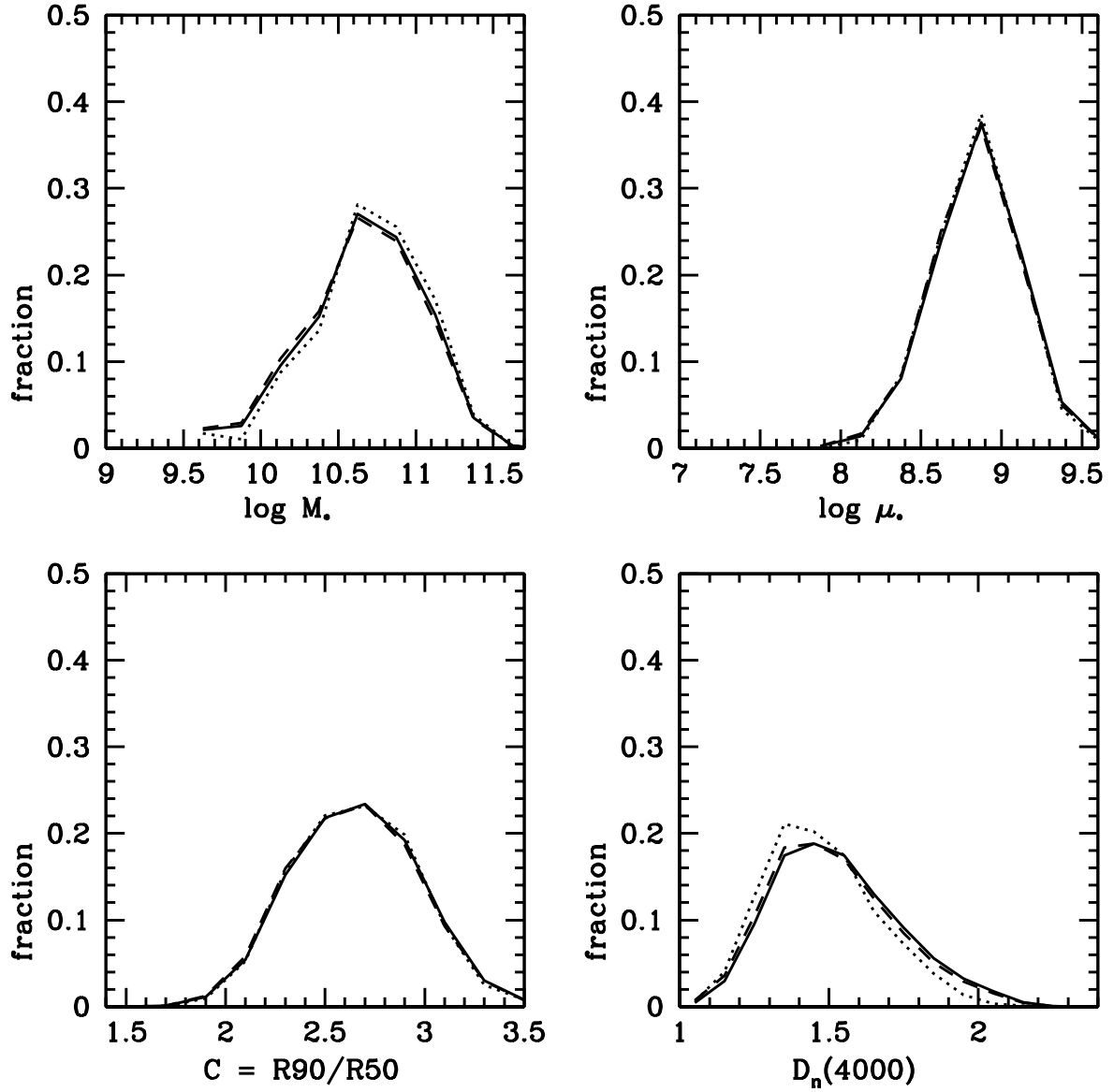


Fig. 4.— The distributions of the total volume-weighted [OIII] luminosity in Type 2 AGN over  $\log M_*$ ,  $\log \mu_*$ ,  $C$ , and  $D_n(4000)$ . The description of the line types is the same as in Fig. 1.

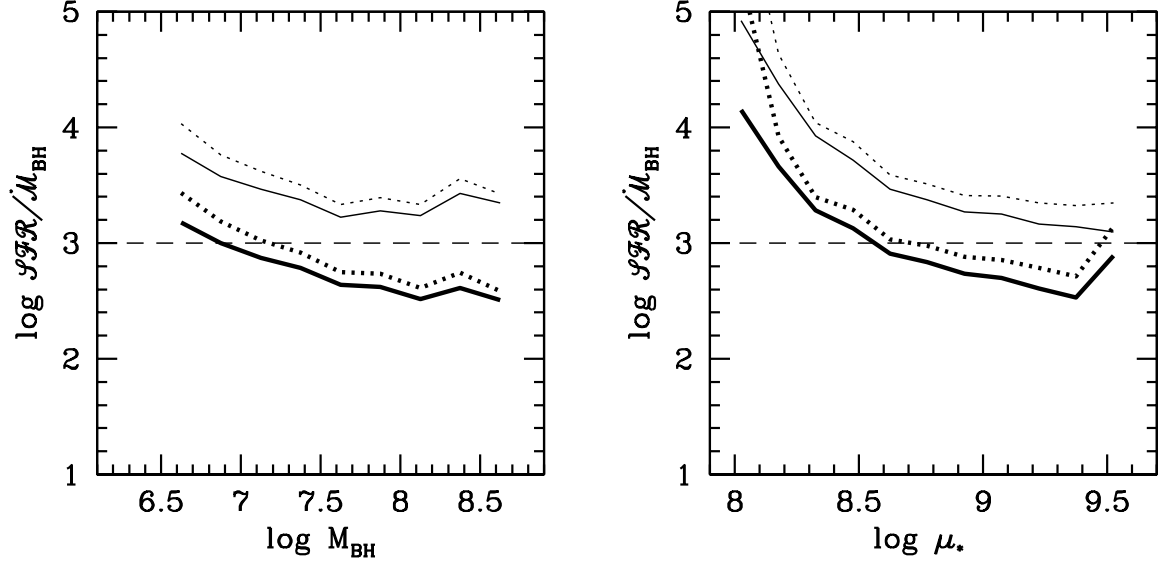


Fig. 5.— The ratio of the total volume-weighted star formation rate in galaxies to the total volume-weighted accretion rate onto black holes as traced by Type 2 AGN is plotted as a function of the black hole mass and the galaxy stellar surface mass density. The thick black lines show the result if SFR is calculated within the fiber aperture for each galaxy and the thin black lines show the result using estimates of *total* SFR. The dotted lines show results restricted to the AGN with  $\log L_{O3} > 10^{6.5} L_{\odot}$ . The dashed line shows the fiducial value of stellar to black hole mass in bulges and elliptical galaxies.



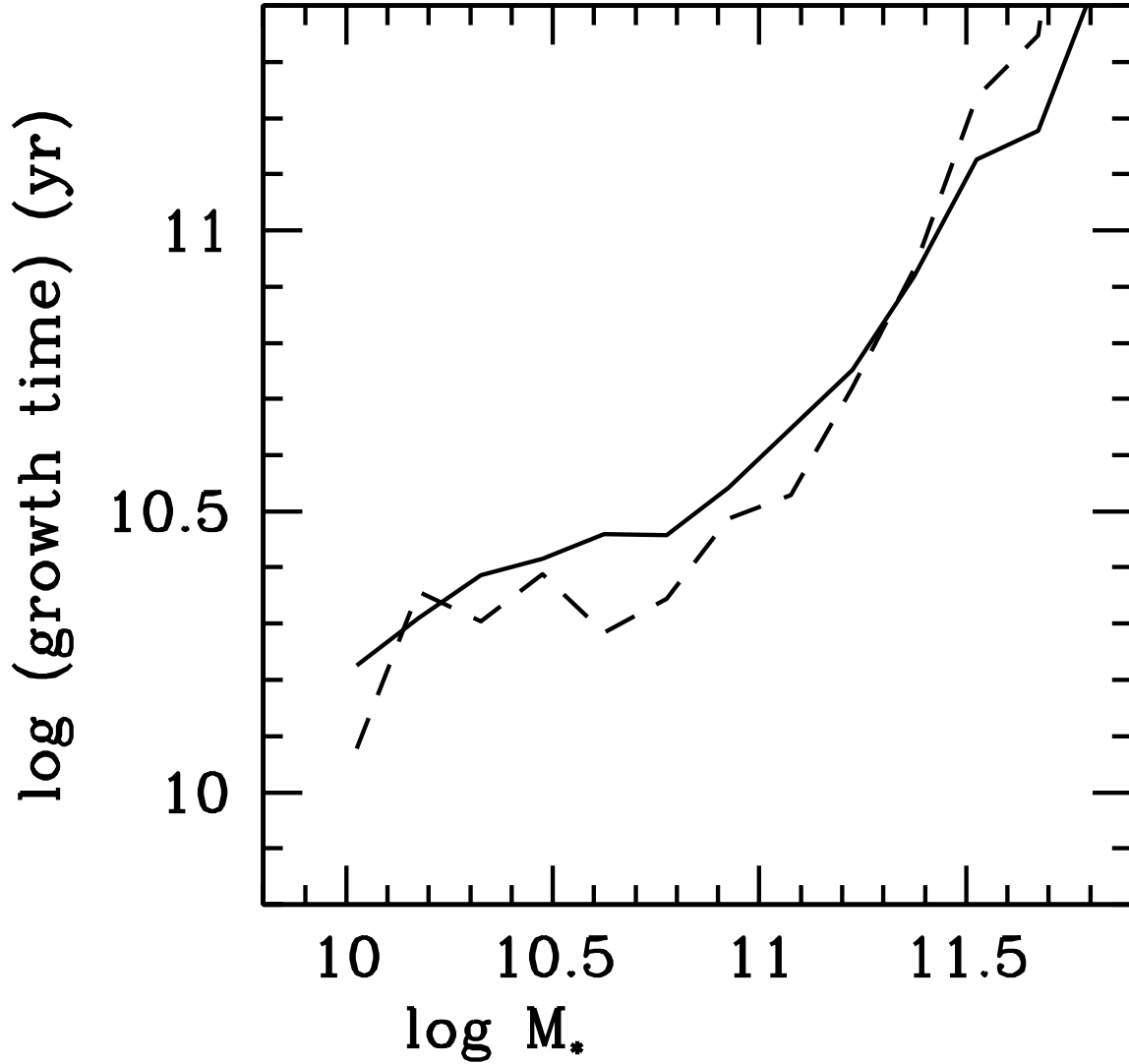


Fig. 6.— The volume-averaged growth time of the galaxy population calculated within the SDSS fiber aperture (solid) is compared with that of the black hole population (dashed). Results have been plotted as a function of galaxy mass. Only AGN with  $\log L_{O3} > 10^{6.5} L_{\odot}$  have been included in the estimation of black hole growth.